Improving Controllability and Plug-and-Play Operation of Wind Farms using B2B Converters

Tomonori Sadamoto and Aranya Chakrabortty

***Abstract*—We show that a critical factor deciding the controllability of a doubly-fed induction generator (DFIG) in a wind power system is the ratio of its leakage reactance to resistance. If this ratio is high then the DFIG has two uncontrollable slow resonant modes. In that situation any type of control action for attenuating disturbances inside the wind farm becomes impossible. In order to prevent this uncontrollability, we propose to add a back-to-back (B2B) converter in the stator line of the DFIG. This new converter has two benefits - first, it improves the controllability of the wind farm significantly, and second, its signal-flow diagram reveals a cascade structure where the grid is shown to impact the DFIG dynamics, but not vice versa. The cascade structure also enables one to design controllers for regulating the DFIG currents and its DC-link voltages in a completely modular and plug-and-play fashion. We illustrate various implementation aspects of this control mechanisms via numerical simulations of the IEEE 68-bus power system model with one wind farm.**

***Index Terms*—DFIG, Stability, Controllability, Plug-and-Play Control, Wind Power**

I. Introduction

A vast amount of research has been done over the past two decades on the topic of wind energy integration [1]. Starting from detailed modeling of wind turbines and doubly-fed induction generators (DFIG) [2], series of papers have been written on transient stability [3], small-signal stability [4], and control [5], [6] of wind power systems. These control designs are based on ideal models of DFIGs whose model parameters are chosen to ensure strong controllability.

In reality, however, the choice of stator impedances and rotor impedances in a DFIG often results in poor controllability, making it very difficult for the wind farm to impart desired amounts of damping control actions on the power flows on the grid side. Controllability issues for wind power regulation have been reported in several venues such as [7], [8] but only either in the context of steady-state power dispatch or mechanical control of turbine components. To the best of our knowledge, no paper has so far reported the influence of model parameters on the controllability of a DFIG and an wind farm, and in turn, the controllability of an entire wind farm.

In this paper, we show that a critical factor deciding controllability of a DFIG is the ratio of its leakage reactance to resistance. If this ratio is high then the first two slow resonant modes become uncontrollable while the two fast modes become slow but controllable. In this case, any type of control, whether it be for damping, frequency regulation, or disturbance attenuation, becomes very difficult. To resolve this uncontrollability issue, we propose to add a back-to-back (B2B) converter in the stator line of the DFIG. This new converter is shown to have two benefits - first, it improves the controllability of the wind farm significantly, and second, its signal-flow diagram reveals a cascade structure where the grid is shown to impact the DFIG dynamics, but the DFIG states do not feedback to the grid. Thus, the grid becomes insensitive and resilient to any disturbance inside the wind farm. Moreover, any controller meant to regulate the DFIG currents and the DC-link voltage can now be designed in a completely modular and plug-and-play (PnP) fashion by exploiting this cascade property. This PnP property enables us to retune/redesign the controllers without taking into account the dynamics of the rest of the grid, while theoretically guaranteeing the entire system stability. This property is especially useful since with rapidly increasing number of wind farms availability of accurate power system models is becoming difficult, due to which power system operators are inclining towards PnP controllers that can be designed independently from the rest of the grid. It also preserves grid stability whenever a new wind farm is added without requiring any retuning of the existing control gains. PnP control of power-electronic converters has been reported in recent papers such as [9], [10] for the control of microgrids, and has been experimentally shown for B2B converters in papers such as [11]. However, the use of PnP property for providing resilience to the grid against parametric resonance of wind farms, has not been reported yet. Our design provides a theoretical bridge to fulfill this gap. We illustrate various implementation aspects of the controller via numerical simulations using the IEEE 68-bus model with one wind farm.

The rest of this paper is organized as follows. In Section II, we analyze the stability and controllability of a DFIG. In Section III, we numerically show how lack of controllability limits the control performance of an entire wind farm. In Section IV, we propose to add a B2B converter to the stator line of the DFIG. In Section IV-B, we investigate the effectiveness of the proposed approach using the IEEE 68-bus power system with a wind farm. Section V shows concluding remarks.

Notation: We denote the imaginary unit by $j := \sqrt{-1}$. All variables with superscript * denote setpoints (e.g.,$\psi_{\rm ds}^\star$ is the setpoint reference for $\psi_{\rm ds}$). The variables used in this paper are in per unit unless otherwise stated. The nonlinear system $\dot{x} = f(x,u)$, where u is input, is said to be stable if there

This research was supported by CREST, JST Grant Number JPMJCR15K1, Japan. Work of the second author was partially supported by the US National Science Foundation under grant ECS 1711004.

T. Sadamoto is with the Department of Mechanical and Intelligent Systems Engineering, Graduate School of Informatics and Engineering, The University of Electro-Communications; 1-5-1, Chofugaoka, Chofu, Tokyo 182-8585, Japan. Email: sadamoto@uec.ac.jp.

A. Chakrabortty is with the Electrical & Computer Engineering, North Carolina State University; Raleigh, North Carolina, USA, 27695. Email: achakra2@ncsu.edu

exists an equilibrium $(x^\star, u^\star)$ such that $x(t)$ under $u = u^\star$ asymptotically converges to $x^\star$ as $t \to \infty$.

II. Stability and Controllability Analysis of DFIG

The dynamics of the DFIG plays a central role in the controllability of wind farms. We, therefore, first recall the state-space representation of a standard and widely accepted DFIG model [2], [11], [12]. The dynamics of its stator and rotor flux linkages, are expressed in a rotating d-q reference frame, as

$$\Sigma_{\text{DFIG}}: \ \dot{\psi} = A_\psi(\omega_{\text{h}})\psi + B_{\psi\text{r}} v_{\text{r}} + B_{\psi\text{s}} v_s \tag{1}$$

where $\psi := [\psi_{\text{dr}}, \psi_{\text{qr}}, \psi_{\text{ds}}, \psi_{\text{qs}}]^{\mathsf{T}}, v_{\text{r}} := [v_{\text{dr}}, v_{\text{qr}}]^{\mathsf{T}}, v_{\text{s}} := [v_{\text{ds}}, v_{\text{qs}}]^{\mathsf{T}}$ and

$$A_\psi(\omega_{\text{h}}) := \begin{bmatrix} -\frac{r_{\text{r}} x_{\text{s}}}{\beta} & 1-\omega_{\text{h}} & \frac{r_{\text{r}} x_{\text{m}}}{\beta} & 0 \\ \omega_{\text{h}} - 1 & -\frac{r_{\text{r}} x_{\text{s}}}{\beta} & 0 & \frac{r_{\text{r}} x_{\text{m}}}{\beta} \\ \frac{r_{\text{s}} x_{\text{m}}}{\beta} & 0 & -\frac{r_{\text{s}} x_{\text{r}}}{\beta} & 1 \\ 0 & \frac{r_{\text{s}} x_{\text{m}}}{\beta} & -1 & -\frac{r_{\text{s}} x_{\text{r}}}{\beta} \end{bmatrix}$$

$$B_{\psi r} := \begin{bmatrix} 1 & 0 & 0 & 0 \\ 0 & 1 & 0 & 0 \end{bmatrix}^{\mathsf{T}}, \quad B_{\psi s} = \begin{bmatrix} 0 & 0 & 1 & 0 \\ 0 & 0 & 0 & 1 \end{bmatrix}^{\mathsf{T}} \tag{2}$$

with

$$x_{\text{s}} := x_{\text{m}} + x_{\text{ls}}, \quad x_{\text{r}} := x_{\text{m}} + x_{\text{lr}}, \quad \beta := x_{\text{s}} x_{\text{r}} - x_{\text{m}}^2. \tag{3}$$

In (1)-(3), ω_{h} is the rotor speed, x_{m} is the magnetizing reactance, x_{ls} and x_{lr} are the leakage reactance of the stator and rotor, r_{s} and r_{r} are the resistance of the stator and rotor. Subscripts d, q, s, and r respectively denote d-axis, q-axis, stator and rotor variables. For example, ψ_{dr} is the d-axis rotor flux linkage, and v_{qs} is the q-axis stator voltage. Papers such as [2] show that $x_{\text{ls}} \approx x_{\text{lr}}$ and $r_{\text{s}} \approx r_{\text{r}}$. Based on this observation, to simplify analysis in the following derivation we assume that $x_{\text{ls}} = x_{\text{lr}}$ and $r_{\text{s}} = r_{\text{r}}$. This assumption is made only to simplify calculations. Under the assumption, the DFIG model linearized around $\omega_{\text{h}} = 1$ pu (synchronous speed), can be written as

$$\hat{\Sigma}_{\text{DFIG}}: \ \dot{\hat{\psi}} = \hat{A}_\psi \hat{\psi} + B_{\psi\text{r}} \hat{v}_{\text{r}} + B_{\psi\text{s}} \hat{v}_{\text{s}} + B_\omega \hat{\omega}_{\text{h}} \tag{4}$$

with

$$\hat{A}_\psi := \begin{bmatrix} -\frac{1+\delta}{\tau} & 0 & \frac{1}{\tau} & 0 \\ 0 & -\frac{1+\delta}{\tau} & 0 & \frac{1}{\tau} \\ \frac{1}{\tau} & 0 & -\frac{1+\delta}{\tau} & 1 \\ 0 & \frac{1}{\tau} & -1 & -\frac{1+\delta}{\tau} \end{bmatrix}, \ B_\omega := \begin{bmatrix} -1 \\ 1 \\ 0 \\ 0 \end{bmatrix} \tag{5}$$

and $B_{\psi r}$ and $B_{\psi s}$ in (2), where δ and τ are defined as

$$\delta := \left(\frac{x_{\text{ls}} + x_{\text{lr}}}{2}\right)\frac{1}{x_{\text{m}}}, \quad \tau := \left(\frac{2}{r_{\text{s}} + r_{\text{r}}}\right)\frac{\beta}{x_{\text{m}}}. \tag{6}$$

The variables $\hat{\psi}$, $\hat{v}_{\text{r}}$, $\hat{v}_{\text{s}}$, and $\hat{\omega}_{\text{h}}$ denote deviations from their steady-state values. The following two findings follow from the model (4)-(5):

1) δ-dependency: Note that the parameter δ appears in only the diagonal elements of $\hat{A}_\psi$, and that the four diagonal elements are identical. This implies that each element of $\hat{\psi}$ is driven by a self-feedback term that shifts the four eigenvalues of $\hat{A}_\psi$ uniformly to the left. However, since the leakage reactances x_{ls} and x_{lr} are usually much smaller than the magnetizing reactance x_{m}, $\delta \ll 1$, and thus the impact of this self-feedback on the DFIG dynamics is not very dominant.

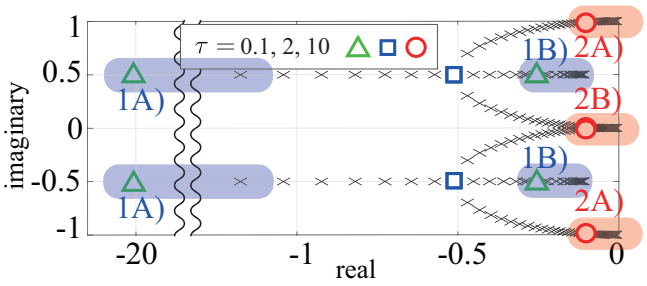

Fig. 1. Variation of the eigenvalues of $\hat{A}_\psi$ in (5) with τ.

2) τ-dependency: The following two cases are considered.

- Case 1 (if $\tau \ll 1$): For the following argument, we define

$$\hat{\psi}_{1\text{A}} := [\hat{\psi}_{\text{dr}} - \hat{\psi}_{\text{ds}}, \hat{\psi}_{\text{qr}} - \hat{\psi}_{\text{qs}}]^{\mathsf{T}}, \hat{\psi}_{1\text{B}} := [\hat{\psi}_{\text{dr}} + \hat{\psi}_{\text{ds}}, \hat{\psi}_{\text{qr}} + \hat{\psi}_{\text{qs}}]^{\mathsf{T}}. \tag{7}$$

Let T be such that $[\hat{\psi}_{1\text{A}}^{\mathsf{T}}, \hat{\psi}_{1\text{B}}^{\mathsf{T}}]^{\mathsf{T}} = T\hat{\psi}$. Then, it follows that

$$T\hat{A}_\psi T^{-1} = \begin{bmatrix} -\frac{\delta+2}{\tau} & \frac{1}{2} & 0 & -\frac{1}{2} \\ -\frac{1}{2} & -\frac{\delta+2}{\tau} & \frac{1}{2} & 0 \\ 0 & -\frac{1}{2} & -\frac{\delta}{\tau} & \frac{1}{2} \\ \frac{1}{2} & 0 & -\frac{1}{2} & -\frac{\delta}{\tau} \end{bmatrix}. \tag{8}$$

From the Gershgorin circle Theorem, two eigenvalues of $T\hat{A}_\psi T^{-1}$ lie in $|\lambda + \frac{\delta+2}{\tau}| \leq 1$ and the other two lie in $|\lambda + \frac{2}{\tau}| \leq 1$. Since $\tau \ll 1$, the first two are fast and their associated state variables are $\hat{\psi}_{1\text{A}}$. Thus, $\hat{\psi}_{\text{dr}} \approx \hat{\psi}_{\text{ds}}$ and $\hat{\psi}_{\text{qr}} \approx \hat{\psi}_{\text{qs}}$, i.e, the behavior of $\hat{\psi}_{\text{dr}}$ (resp. $\hat{\psi}_{\text{qr}}$) and $\hat{\psi}_{\text{ds}}$ (resp. $\hat{\psi}_{\text{qs}}$) will be similar.

- Case 2 (if $\tau \gg 1$): The coupling between $\hat{\psi}_{\text{dr}}$ and $\hat{\psi}_{\text{ds}}$ (or $\hat{\psi}_{\text{qr}}$ and $\hat{\psi}_{\text{qs}}$) is weaker than that between $\hat{\psi}_{\text{ds}}$ and $\hat{\psi}_{\text{qs}}$. Thus, the dynamics of $\hat{\psi}_{\text{dr}}$ (or $\hat{\psi}_{\text{qr}}$) evolve almost independently from the other three fluxes, and this evolution will be stable because of the self-feedback term. The open-loop system, on the other hand, will have a resonance mode. This can be seen easily from the 2×2 lower-right block of $\hat{A}_\psi$ which has eigenvalues $-\frac{1+\delta}{\tau} \pm j$.

As a result of these two findings, the stability and controllability of the DFIG dynamics can be interpreted as follows.

1) Stability: Fig. 1 depicts the variation of these eigenvalues of $\hat{A}_\psi$ in (5) by changing τ in the range of $[0.01, 100]$ for $\delta = 0.0243$.

When $\tau \ll 1$, participation factor analysis [13] of the DFIG model (4)-(5) reveals that $\hat{\psi}_{\text{dr}} - \hat{\psi}_{\text{ds}}$ and $\hat{\psi}_{\text{qr}} - \hat{\psi}_{\text{qs}}$ exhibit fast dynamics, while $\hat{\psi}_{\text{dr}} + \hat{\psi}_{\text{ds}}$ and $\hat{\psi}_{\text{qr}} + \hat{\psi}_{\text{qs}}$ exhibit slow dynamics.

As the value of τ increases, the eigenvalue variation is bifurcated at $\tau = 2$. This corresponds to the situation when the average of the two leakage reactances is close to that of the leakage resistances. To see this, let us define $x_{\text{l}} := x_{\text{ls}} = x_{\text{lr}}$ and $r := r_{\text{s}} = r_{\text{r}}$. Then, the parameter τ can be equivalently written as $\tau = (2+\delta)\frac{x_{\text{l}}}{r}$. Usually, $\delta \approx 0$ because the leakage reactance is much smaller than the magnetizing reactance [11]. Thus, $\tau = 2$ corresponds to $x_{\text{l}} \approx r$.

When $\tau \gg 1$, Fig. 1 shows that the mode 2A) shows an oscillatory behavior with frequency around 1 (rad/sec) while

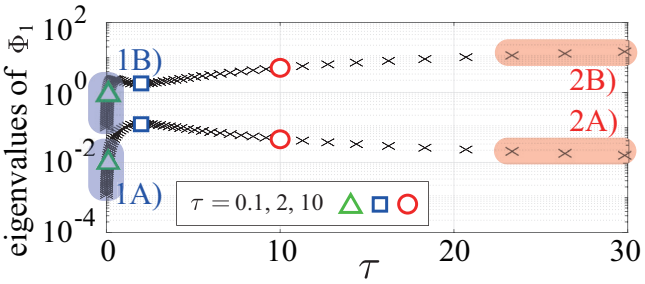

Fig. 2. Variation of the eigenvalues of Φ_1 with τ

the mode 2B) shows slow convergent behavior. Participation factor analysis reveals that each mode is associated with

$$\hat{\psi}_{2\mathrm{A}} := [\hat{\psi}_{\mathrm{ds}}, \hat{\psi}_{\mathrm{qs}}]^{\mathsf{T}}, \quad \hat{\psi}_{2\mathrm{B}} := [\hat{\psi}_{\mathrm{dr}}, \hat{\psi}_{\mathrm{qr}}]^{\mathsf{T}}, \tag{9}$$

respectively. The oscillatory behavior happens because the stator flux $\hat{\psi}_{2\mathrm{A}}$ has a resonance pole, while the slow convergence happens because of weak self-feedback.

2) Controllability: Control actions in a DFIG are typically applied by regulating the rotor voltage v_{r} through a rotor-side converter [11]. Therefore, in the following controllability analysis we consider v_{r} as the main control input. This covers the case when $\hat{\omega}_{\mathrm{h}}$ is the control input as both $\hat{\omega}_{\mathrm{h}}$ and v_{r} affect $\hat{\psi}_{\mathrm{dr}}$ and $\hat{\psi}_{\mathrm{qr}}$.

The controllability of the DFIG model (4)-(5) from $\hat{v}_{\mathrm{r}}$ can be quantified by the eigenvalues of the controllability gramian $\Phi_1 := \int_0^\infty e^{\hat{A}_\psi t} B_{\psi r} (e^{\hat{A}_\psi t} B_{\psi r})^{\mathsf{T}} dt$. Fig. 2 shows the variation of the eigenvalues of this gramian with changes in τ. Note that two eigenvalues are overlapped at all marks. When $\tau \ll 1$, the state $\hat{\psi}_{1\mathrm{A}}$ in (7) is seen to be less controllable than $\hat{\psi}_{1\mathrm{B}}$ because $\hat{\psi}_{1\mathrm{A}}$ converges to its steady-state very fast. When $\tau \gg 1$, the state $\hat{\psi}_{2\mathrm{A}}$ in (9) is less controllable than the rotor flux. This is because the large value of τ makes the coupling between the stator dynamics and the rotor dynamics driven by the control input $\hat{v}_{\mathrm{r}}$ weak.

In summary, we can write the following observations about the stability and controllability of the DFIG model. Note that τ can be written as $\tau = (2+\delta)x_{\mathrm{l}}/r$.

Case 1, when $x_{\mathrm{l}} \ll r$: The slow and resonant state $\hat{\psi}_{1\mathrm{A}}$ in (7) is controllable. The other state $\hat{\psi}_{1\mathrm{B}}$ is less controllable, but is fast. Thus, in terms of stabilization of the DFIG dynamics, this case is not very problematic.

Case 2, when $x_{\mathrm{l}} \gg r$: The slow state $\hat{\psi}_{2\mathrm{B}}$ in (9) is controllable. However, the state $\hat{\psi}_{2\mathrm{A}}$ is less controllable even though the mode 2A) has a resonant pole. Thus, this case will cause a problem for stabilization and transient performance of the DFIG.

We end this section with a simulation result for the non-ideal case when $x_{\mathrm{ls}} \neq x_{\mathrm{lr}}$, $r_{\mathrm{s}} \neq r_{\mathrm{r}}$, $\omega_{\mathrm{h}}^\star \neq 1$. For this we assume the parameters of Σ_{DFIG} in (1) to lie in the following ranges: $x_{\mathrm{m}} \in [177.6395, 217.6395]$, $x_{\mathrm{ls}} \in [2.62, 6.62]$, $x_{\mathrm{lr}} \in [2.976, 6.976]$, $r_{\mathrm{s}} \in [0.0440, 0.444]$, $r_{\mathrm{r}} \in [0.0745, 0.4745]$. The mean values of each range are the DFIG model parameters provided in [2] rated at 100MVA. Let $\omega_{\mathrm{h}}^\star \in [0.9, 1.1]$. Note that the Jacobian of $A_\psi(\omega_{\mathrm{h}})$ at $\omega_{\mathrm{h}}^\star$ coincides with $A_\psi(\omega_{\mathrm{h}}^\star)$. We denote the eigenvalues of $A_\psi(\omega_{\mathrm{h}}^\star)$ by λ_{2A}, λ_{2B}, and their conjugates. Without loss of generality, the imaginary parts of λ_{2A} and λ_{2B} are assumed to be non-negative. The ranges of their values for 1000 combinations of linearization points chosen from the respective parameter ranges, together with

Eigenvalues for 1000 trials	Typical eigenvectors
$\mathrm{Re}(\lambda_{2\mathrm{A}}) \in [-0.067, -0.004]$ $\mathrm{Im}(\lambda_{2\mathrm{A}}) \in [0.995, 1.000]$	$\begin{bmatrix} -0.0068 \\ -0.0001 \\ 0.0000 \\ 0.7071 \end{bmatrix} + j \begin{bmatrix} 0.0001 \\ 0.0068 \\ 0.7071 \\ 0.0000 \end{bmatrix}$
$\mathrm{Re}(\lambda_{2\mathrm{B}}) \in [-0.082, -0.006]$ $\mathrm{Im}(\lambda_{2\mathrm{B}}) \in [0, 0.1]$	$\begin{bmatrix} 0.0000 \\ 0.7068 \\ 0.0210 \\ 0.0004 \end{bmatrix} + j \begin{bmatrix} 0.7068 \\ 0.0000 \\ 0.0004 \\ 0.0210 \end{bmatrix}$

TABLE I
THE RANGE OF THE EIGENVALUES OF $A_\psi(\omega_{\mathrm{h}}^\star)$ FOR 1000 TRIALS AND THE TYPICAL VALUES OF THEIR EIGENVECTORS.

Eigenvalues for 1000 trials	Typical eigenvectors
$\sigma_{2\mathrm{A},1} \in [0.0015, 0.0335]$ $\sigma_{2\mathrm{A},2} \in [0.0015, 0.0335]$	$\begin{bmatrix} 0.0296 \\ -0.0011 \\ -0.0024 \\ 0.9996 \end{bmatrix}, \begin{bmatrix} 0.0011 \\ 0.0296 \\ -0.9996 \\ -0.0024 \end{bmatrix}$
$\sigma_{2\mathrm{B},1} \in [6.1926, 81.1249]$ $\sigma_{2\mathrm{B},2} \in [6.1926, 81.1249]$	$\begin{bmatrix} 0.9987 \\ -0.0405 \\ 0.0000 \\ -0.0296 \end{bmatrix}, \begin{bmatrix} 0.0405 \\ 0.9987 \\ 0.0296 \\ 0.0000 \end{bmatrix}$

TABLE II
THE RANGE OF THE EIGENVALUES OF Φ_1 FOR 1000 TRIALS AND THE TYPICAL VALUES OF THEIR EIGENVECTORS.

the associated eigenvectors are listed in Table I. Similarly, the range of eigenvalues of the controllability gramian Φ_1 and their eigenvectors are listed in Table II, where the eigenvalues are denoted as $\sigma_{2\mathrm{A},i}$ and $\sigma_{2\mathrm{B},i}$ for $i \in \{1, 2\}$. The results show that the stability and controllability properties of the DFIG under the non-ideal scenario follows the same trend as enumerated in Case 1 and Case 2 above.

So far, we have analyzed the controllability of a DFIG as an isolated component. Next we show how the stability and controllability of a DFIG influences the stabilization of an entire wind farm connected to the grid.

III. Impact of DFIG Resonance and Controllability on A Wind Farm

A wind farm consists of multiple wind generators. Using standard practice [14], we consider the model of all the generators to be the same, as a result of which the wind farm is modeled as a single wind generator whose model is identical to that of each generator, and the total injection power is the sum of the power output of individual generators. The aggregated model consists of a wind turbine, a DFIG, and a back-to-back (B2B) converter. The B2B converter consists of a rotor-side converter (RSC), a grid-side converter (GSC), and their respective inner-loop and outer-loop controllers. Please see [15] for the detail about the wind farm dynamics.

To illustrate the impact of resonance and controllability on this wind farm model, we consider the farm to be connected to an infinite bus through a purely reactive transmission line with impedance x. From Kirchoff's law, it follows that

$$V_{\mathrm{d}} + jV_{\mathrm{q}} = \bar{V}_{\mathrm{d}} + j\bar{V}_{\mathrm{q}} - jx(i_{\mathrm{d}} + ji_{\mathrm{q}}) \tag{10}$$

where $V_{\mathrm{d}} + jV_{\mathrm{q}}$ is the wind bus voltage, $\bar{V}_{\mathrm{d}} + j\bar{V}_{\mathrm{q}}$ is the infinite bus voltage, and $i_{\mathrm{d}} + ji_{\mathrm{q}}$ is the net current injecting from the wind farm. We simulate the dynamic performance of this one-machine-infinite-bus power system in response to a fault. Let $x = 0.01$ in (10), $\bar{V}_{\mathrm{d}} = 0.9934$, $\bar{V}_{\mathrm{q}} = 0.1147$, and the number of wind generators inside the farm be 60. The other model parameters are shown in [15]. We suppose the system to be in an equilibrium for $t < 0$. At $t = 0$ a fault happens, whose effect is modeled by an impulsive change

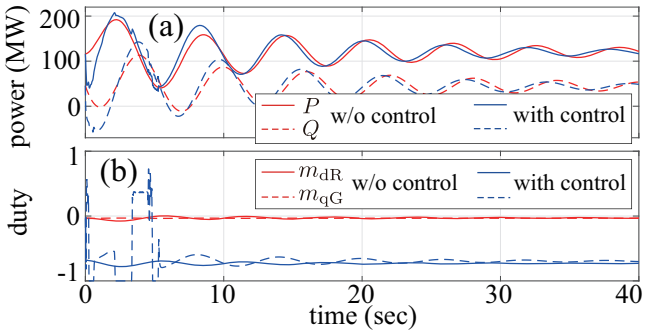

Fig. 3. The trajectories of (a) active and reactive power injected by the wind farm, denoted as P and Q respectively, and (b) the d-axis duty cycle of the RSC and the q-axis duty cycle of the GSC, denoted as m_{dR} and m_{qG} respectively.

in the DFIG current from its equilibrium. The red solid and dotted lines in Fig. 3(a) show the active and reactive power injected by the wind farm to the grid. The respective lines in Fig. 3(b) show the d-axis duty cycle of the RSC and the q-axis duty cycle of the GSC. The responses shown in Fig. 3(a) are oscillatory with a frequency around 1 (rad/sec) that arises from the resonance mode of the DFIG. Clearly, the internal controllers of both RSC and GSC fail to damp this oscillation. To investigate whether a supplementary controller can fulfill this goal, we consider controlling both the RSC and GSC. Let the control input be denoted as $u \in \mathbb{R}^4$ where its first two elements are the additional signals to the d- and q-axis duty cycles of RSC while the last two are those of the GSC. A state feedback control $u = K(x - x^\star)$ is applied to the system, where $x \in \mathbb{R}^{16}$ denotes the wind farm state, and K is designed to minimize $J = \int_0^\infty w\|\hat{\psi}(t)\|^2 + \|u(t)\|^2 dt$ with a scalar weight w, where $\hat{\psi}$ is defined in (4). In Fig. 3(a)-(b), blue lines show the case when the optimal controller with $w = 10^4$ is used. By comparing the blue and red lines in Fig. 3(a), it can be seen that the resonant oscillations in the power outputs are still poorly damped. Furthermore, Fig. 3(b) shows that the duty cycles under this optimal control are often saturated because of the lack of controllability. Although these simulations are based on an aggregated wind farm model, a similar trend follows for non-aggregated wind farm consisting of heterogeneous wind generators.

These results show that the uncontrollability of the resonant mode significantly influences the wind farm dynamics. Motivated by these observations, we next propose a way to increase the controllability of the resonant modes.

IV. Proposed Approach

A. Benefits of Adding B2B Converter to Stator Line

To overcome the problem described above, we propose to add a second B2B converter to the stator line of the DFIG, as shown in Fig. 4(a). We refer to the AC/DC and DC/AC converters as stator-side converter (SSC) and bus-side converter (BSC), respectively. The model of the second B2B converter is described in Table III. Two main advantages of adding this second B2B converter are summarized as follows.

1) Improvement of Controllability: To show that (11)-(16) improves the controllability of DFIG in (1), we impose the following assumption:

Assumption 1: The duty cycles of the RSC, GSC, SSC, and BSC are not saturated at any time t during the time of interest.

• BSC:

$$\begin{aligned}
\tfrac{L'_{\mathrm{G}}}{\bar{\omega}}\dot{i}'_{\mathrm{dG}} &= -R'_{\mathrm{G}}i'_{\mathrm{dG}} + L'_{\mathrm{G}}i'_{\mathrm{qG}} + V_{\mathrm{d}} - \tfrac{m'_{\mathrm{dG}}}{2}v'_{\mathrm{dc}},\\
\tfrac{L'_{\mathrm{G}}}{\bar{\omega}}\dot{i}'_{\mathrm{qG}} &= -R'_{\mathrm{G}}i'_{\mathrm{qG}} - L'_{\mathrm{G}}i'_{\mathrm{dG}} + V_{\mathrm{q}} - \tfrac{m'_{\mathrm{qG}}}{2}v'_{\mathrm{dc}},\\
P_{\mathrm{s}} + jQ_{\mathrm{s}} &= -\gamma(V_{\mathrm{d}}i'_{\mathrm{dG}} + V_{\mathrm{q}}i'_{\mathrm{qG}}) - j\gamma(V_{\mathrm{q}}i'_{\mathrm{dG}} - V_{\mathrm{d}}i'_{\mathrm{qG}}).
\end{aligned} \tag{11}$$

where i'_{dG} and i'_{qG} are the d- and q-axis current flowing from the grid side to the BSC, m'_{dG} and m'_{qG} are the d- and q-axis duty cycles defined in (13), V_{d} and V_{q} are the d- and q-axis bus voltage, v'_{dc} is the dc-link voltage defined in (16), $P_{\mathrm{s}} + jQ_{\mathrm{s}}$ is the power injecting from the converter, $\bar{\omega}$ is the synchronous speed (60Hz), L'_{G} and R'_{G} are the inductance and resistance of the converter, and γ is the number of wind generators inside the farm.

• Outer-Loop controller of BSC:

$$\dot{\zeta}'_{\circ\mathrm{G}} = K'_{\mathrm{I},\circ\mathrm{G}}(\alpha'_\circ - \alpha'^\star_\circ), \quad i'^{\mathrm{ref}}_{\circ\mathrm{G}} = K'_{\mathrm{P},\circ\mathrm{G}}(\alpha'_\circ - \alpha'^\star_\circ) + \zeta'_{\circ\mathrm{G}} \tag{12}$$

for $\circ \in \{\mathrm{d},\mathrm{q}\}$, where $\alpha'_{\mathrm{d}} := P_{\mathrm{s}}$, $\alpha'_{\mathrm{q}} := Q_{\mathrm{s}}$, $\zeta'_{\circ\mathrm{G}}$ is the controller state, $i'^{\mathrm{ref}}_{\circ\mathrm{G}}$ is the reference signal of $i'_{\circ\mathrm{G}}$, $K'_{\mathrm{I},\circ\mathrm{G}}$ and $K'_{\mathrm{P},\circ\mathrm{G}}$ are the integral and proportional gains of the controller.

• Inner-Loop controller of BSC:

$$\begin{aligned}
\tau'_{\mathrm{G}}\dot{\chi}'_{\circ\mathrm{G}} &= i'^{\mathrm{ref}}_{\circ\mathrm{G}} - i'_{\circ\mathrm{G}},\\
m'_{\circ\mathrm{G}} &= \mathrm{sat}\left(\tfrac{2}{v'_{\mathrm{dc}}}\left(\tilde{V}'_\circ - R'_{\mathrm{G}}\chi'_{\circ\mathrm{G}} - \tfrac{L'_{\mathrm{G}}}{\bar{\omega}\tau'_{\mathrm{G}}}(i'^{\mathrm{ref}}_{\circ\mathrm{G}} - i'_{\circ\mathrm{G}}) + u'_{\circ\mathrm{G}}\right)\right),
\end{aligned} \tag{13}$$

for $\circ \in \{\mathrm{d},\mathrm{q}\}$ where $\tilde{V}'_{\mathrm{d}} := V_{\mathrm{d}} + L'_{\mathrm{G}}i'_{\mathrm{qG}}$, $\tilde{V}'_{\mathrm{q}} := V_{\mathrm{q}} - L'_{\mathrm{G}}i'_{\mathrm{dG}}$, $\chi'_{\circ\mathrm{G}}$ is the controller state, $i'_{\circ\mathrm{G}}$ is defined in (11), $i'^{\mathrm{ref}}_{\circ\mathrm{G}}$ is in (12), v'_{dc} is in (16), $u'_{\circ\mathrm{G}}$ is the control input, τ'_{G} is the designed time constant of the BSC current dynamics, and $\mathrm{sat}(\cdot)$ is the saturation function whose output is restricted within [-1,1].

• SSC

$$v_{\mathrm{ds}} = \frac{m'_{\mathrm{dR}}}{2}v'_{\mathrm{dc}}, \quad v_{\mathrm{qs}} = \frac{m'_{\mathrm{qR}}}{2}v'_{\mathrm{dc}}, \tag{14}$$

where m'_{dR} and m'_{qR} are defined in (15), v'_{dc} is in (16).

• Inner-Loop controller of SSC:

$$\begin{aligned}
\dot{\chi}'_{\circ\mathrm{R}} &= \kappa'_{\mathrm{I},\circ\mathrm{R}}(i_{\circ\mathrm{s}} - i^\star_{\circ\mathrm{s}}),\\
m'_{\circ\mathrm{R}} &= \mathrm{sat}\left(\tfrac{2}{v'_{\mathrm{dc}}}\left(\kappa'_{\mathrm{P},\circ\mathrm{R}}(i_{\circ\mathrm{s}} - i^\star_{\circ\mathrm{s}}) + \chi'_{\circ\mathrm{R}} + u'_{\circ\mathrm{R}}\right)\right)\\
i_{\mathrm{ds}} &= \tfrac{1}{\beta}(x_{\mathrm{m}}\psi_{\mathrm{dr}} - x_{\mathrm{r}}\psi_{\mathrm{ds}}), \quad i_{\mathrm{qs}} = \tfrac{1}{\beta}(x_{\mathrm{m}}\psi_{\mathrm{qr}} + x_{\mathrm{r}}\psi_{\mathrm{qs}})
\end{aligned} \tag{15}$$

for $\circ \in \{\mathrm{d},\mathrm{q}\}$, where $\chi'_{\circ\mathrm{R}}$ is the controller state, $u'_{\circ\mathrm{R}}$ is the control input, v'_{dc} is in (16), $\psi_{\circ\circ}$ is in (1), x_{m}, x_{r} and β are in (3), $\kappa'_{\mathrm{I},\circ\mathrm{R}}$ and $\kappa'_{\mathrm{P},\circ\mathrm{R}}$ are the integral and proportional gains of the controller.

• DC-link:

$$\begin{aligned}
\tfrac{C'_{\mathrm{dc}}}{\bar{\omega}}\dot{v}'_{\mathrm{dc}} &= \tfrac{1}{v'_{\mathrm{dc}}}\left(V_{\mathrm{d}}i'_{\mathrm{dG}} + V_{\mathrm{q}}i'_{\mathrm{qG}} + v_{\mathrm{ds}}i_{\mathrm{ds}}\right.\\
&\qquad \left. + v_{\mathrm{qs}}i_{\mathrm{qs}} - R'_{\mathrm{G}}(i'^2_{\mathrm{dG}} + i'^2_{\mathrm{qG}})\right) - G'_{\mathrm{sw}}v'_{\mathrm{dc}},
\end{aligned} \tag{16}$$

where i'_{dG} and i'_{qG} are defined in (11), i_{ds} and i_{qs} are in (15), v_{ds} and v_{qs} are in (1), C'_{dc} is the dc-link capacitance, and G'_{sw} is the conductance representing the switching loss of the B2B converter.

TABLE III
The dynamics of the second B2B converter.

Under this assumption, by substituting (15) into (14), we have

$$v_{\circ\mathrm{s}} = \kappa'_{\mathrm{P},\circ\mathrm{R}}(i_{\circ\mathrm{s}} - i^\star_{\circ\mathrm{s}}) + \chi'_{\circ\mathrm{R}} + u'_{\circ\mathrm{R}}, \quad \circ \in \{\mathrm{d},\mathrm{q}\}, \tag{17}$$

which implies that v_{ds} and v_{qs} can be directly controlled by the inner-loop controller. It follows from (1) that v_{ds} (or v_{qs}) directly drives ψ_{ds} (or ψ_{qs}), which is resonant and less-controllable by the rotor voltage v_{dr} (or v_{qr}). Therefore, we can see that the controllability of ψ_{ds} and ψ_{qs} are improved via v_{ds} and v_{qs}. Let Φ_1 and Φ_2 be the controllability gramians associated with the pairs $(A_\psi(\omega^\star_{\mathrm{h}}), B_{\psi\mathrm{r}})$ and $(A_\psi(\omega^\star_{\mathrm{h}}), [B_{\psi\mathrm{r}}, B_{\psi\mathrm{s}}])$, respectively. The eigenvalues of these two are

$$\begin{aligned}
\sigma(\Phi_1) &= \{0.0122, 0.0122, 17.3210, 17.3210\}\\
\sigma(\Phi_2) &= \{16.9537, 16.9537, 19.8516, 19.8516\},
\end{aligned}$$

which shows that the SSC drastically improves the controllability of the DFIG.

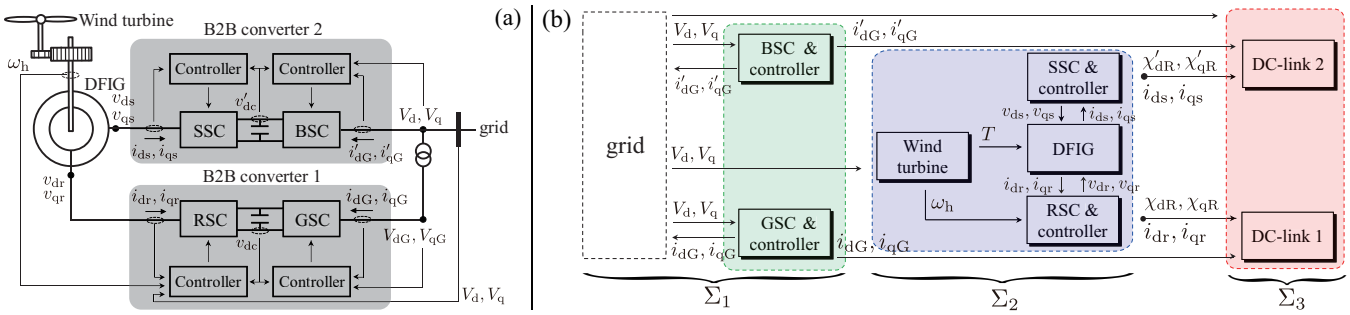

Fig. 4. (a) Physical structure of the wind farm when a second B2B converter is added to the stator line. (b) Signal-flow diagram of the power system with the proposed wind farm as shown in (a). In the subfigure (b), $i_{\rm dG}$ and $i_{\rm qG}$ are the current flowing from the grid to GSC, $i_{\rm dr}$ and $i_{\rm qr}$ are the current flowing from the rotor to RSC, T is the electro-mechanical torque used by the DFIG, $\chi_{\rm dR}$ and $\chi_{\rm qR}$ are the state of the inner-loop controller of RSC. The other symbols are defined in Table III and (1). Furthermore, the external control inputs on the duty cycles are omitted for brevity.

2) Plug-and-Play Operation: The introduction of the B2B also imparts a PnP property for controlling the entire wind farm. This can be shown as follows. Fig. 4(b) shows the signal flow diagram of the closed-loop system including both the wind farm and the grid. Let Σ_1, Σ_2, and Σ_3 denote the subsystems as shown in the figure. The important property of this closed-loop system is its cascade structure, where

p1) Σ_1 affects Σ_2 and Σ_3, but not vice versa, and
p2) Σ_2 affects Σ_3, but not vice versa.

These two facts can be established as follows. By substituting (13) into (11), the BSC dynamics can be rewritten as

$$\frac{L'_{\rm G}}{\bar\omega}\dot i'_{\circ\rm G} = R'_{\rm G}(\chi'_{\circ\rm G} - i'_{\circ\rm G}) + \frac{L'_{\rm G}}{\bar\omega\tau'_{\rm G}}(i'^{\rm ref}_{\circ\rm G} - i'_{\circ\rm G}) - u'_{\circ\rm G} \quad (18)$$

for $\circ \in \{\rm d, q\}$. From (18), it follows that the signal flow between the BSC with its controllers and the DC-link dynamics is a cascade where the former is upstream and the latter is downstream, as shown in the figure. The same argument holds for the three upstream components RSC, GSC, and SSC and their respective downstream DC-links. Thus, p2) holds. Also, note that the outer-loop controller of BSC in (12) and the DC-link dynamics (16) are influenced by the grid dynamics via the bus voltage $[V_{\rm d}, V_{\rm q}]^{\mathsf T}$. Similarly, the controllers of GSC and RSC, and the DC-link dynamics of the first B2B converter are influenced by $[V_{\rm d}, V_{\rm q}]^{\mathsf T}$; see [15] for the details. On the other hand, the bus voltage is driven by the variation of the net injected power, which is determined by the GSC and BSC. Thus, p1) holds.

We next state a theorem to theoretically establish the PnP property imparted by these two cascade structures. Let η_1, η_2, and η_3 denote the state of Σ_1, Σ_2 and Σ_3 in Fig. 4(b), respectively. Let $\eta := [\eta_1^{\mathsf T}, \eta_2^{\mathsf T}, \eta_3^{\mathsf T}]^{\mathsf T}$. Furthermore, we suppose that an equilibrium $\eta^\star$ (or equivalently the triple $\{\eta_1^\star, \eta_2^\star, \eta_3^\star\}$) is given by a standard power flow calculation.

Theorem 1: Let Assumption 1 hold. Suppose that Σ_1 and Σ_3 are stable at $\eta_1^\star$ and $\eta_3^\star$. Then, the following two statements are true.

i) The interconnection of Σ_1, Σ_2, and Σ_3 is stable at $\eta^\star$ for any quadruple $\{\kappa'_{\rm I,dR}, \kappa'_{\rm I,qR}, \kappa'_{\rm P,dR}, \kappa'_{\rm P,qR}\}$ such that Σ_2 at $\eta_2^\star$ is stable, where $\kappa'_{\rm I,dR}$, $\kappa'_{\rm I,qR}$, $\kappa'_{\rm P,dR}$ and $\kappa'_{\rm P,qR}$ are defined in (15).

ii) Let z denote a measurable signal from Σ_2 and Σ_3, i.e., $z = h(\eta_2, \eta_3)$. Consider an output-feedback controller

$$\mathcal{K}: \begin{cases} \dot\zeta = r(\zeta, z) \\ u = s(\zeta, z) \end{cases}, \quad u := [u'_{\rm dR}, u'_{\rm qR}]^{\mathsf T} \quad (19)$$

such that $s(\zeta^\star, z^\star) = u^\star$, and the interconnection of the triple $\{\Sigma_2, \Sigma_3, \mathcal{K}\}$ is stable, where ζ is the state of $\mathcal{K}$, $u'_{\rm dR}$ and $u'_{\rm qR}$ are defined in (15). Then, the overall closed-loop system $\{\Sigma_1, \Sigma_2, \Sigma_3, \mathcal{K}\}$ is stable at $[\eta^{\star\mathsf T}, \zeta^{\star\mathsf T}]^{\mathsf T}$.

Proof 1: Note that the choice of the controller gains $\{\kappa'_{\rm I,dR}, \kappa'_{\rm I,qR}, \kappa'_{\rm P,dR}, \kappa'_{\rm P,qR}\}$ does not change the equilibria of Σ_1, Σ_2, and Σ_3. Note that each of Σ_1, Σ_2, and Σ_3 are stable with respect to their setpoints. Using the result in [16] that a cascade interconnection of multiple nonlinear systems is stable if each system is stable, the claim i) follows. Also, the controller (19) does not change the equilibria because $r(\zeta^\star, z^\star) = 0$ and $s(\zeta^\star, z^\star) = u^\star$. Thus, owing to the cascade structure of Σ_1, Σ_2, and Σ_3, the claim ii) follows.

In this theorem, the claim i) implies that the inner-loop controller of the SSC can be tuned independent of the dynamics of the rest of the system. The claim ii) implies that, if needed, additional control mechanisms can also be added to the components without any influence from the remaining components. For example, one can design an LQR controller by feeding back the stator current and the dc-link voltage, i.e., $z := [i_{\rm ds}, i_{\rm qs}, v'_{\rm dc}]^{\mathsf T}$ for improving the damping performance of Σ_2 and Σ_3. Typically, $i_{\rm ds}$, $i_{\rm qs}$, and $v'_{\rm dc}$ are measurable [11]. Furthermore, a similar claim follows for RSC also. Once the tuning ensures that Σ_2 is stable, there is no need to re-tune these controllers even if the grid dynamics change drastically over time. Therefore, adding the B2B converter to the stator line enables one to manage the wind farm operation in a completely modular and PnP fashion.

B. Numerical Demonstration

We close this section by numerically illustrating the advantages of adding the proposed B2B converter to the stator line of the DFIG. We consider the IEEE 68-bus power system [15] with a single wind farm installed at Bus 22. The topology of the model, tie-line parameters, and machine parameters can be found in [13]. The physical parameters of the second B2B converter (11)-(16) are as follows. $L'_{\rm G} = 63.35$, $R'_{\rm G} = 0.05$, $G'_{\rm sw} = 1.19 \times 10^{-5}$, $C'_{\rm dc} = 44.87$, $K'_{\rm I,dG} = -0.01$, $K'_{\rm I,qG} = 0.01$, $K'_{\rm P,dG} = -0.2$, $K'_{\rm P,qG} = 0.01$, $\kappa'_{\rm I,dG} = 0.01$, $\kappa'_{\rm I,qG} = 0.01$, and $\tau'_{\rm G} = 0.1$. In Fig. 5(a), the red lines show the frequency deviation of all synchronous generators after a fault in the DFIG model (the same fault was considered in Section III). Due to the resonance mode of the DFIG, sustained oscillations around 1 (rad/sec) appear in the frequency deviations. On the other hand, when the second B2B

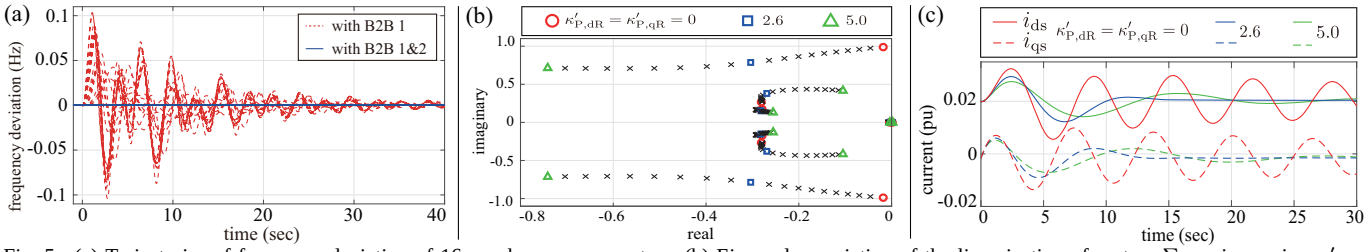

Fig. 5. (a) Trajectories of frequency deviation of 16 synchronous generators. (b) Eigenvalue variation of the linearization of system Σ_2 as increasing $\kappa'_{\mathrm{P,dR}}$ and $\kappa'_{\mathrm{P,qR}}$ in (15). (c) Trajectories of DFIG stator current, where i_{ds} and i_{qs} are defined in (15).

converter is added to the stator line of the DFIG, the same fault is seen to have absolutely no effect on the grid states, as indicated by the blue lines. This decoupling property stems from the justification of the cascade structure of the model. The proposed strategy, therefore, provides complete resilience to grid operation against faults and disturbances in the wind farm. The wind farm owner, however, may still want to control the transient response of Σ_2 and Σ_3. For this, we tune the proportional gain of the inner-loop controller of the SSC in (15). Fig. 5(b) shows the eigenvalues of the closed-loop model of Σ_2 linearized at its equilibrium following from the power flow solution. One can see that the eigenvalue around $0 \pm j1$ (that corresponds to the resonance mode of the DFIG) moves to the left as the proportional gain increases. This is because the SSC controls the stator voltage, by which the resonance mode appearing on the stator flux dynamics is now directly regulated. Fig. 5(b) also shows that high values of the gain excite another mode around $-0.28 \pm j0.5$ when $\kappa'_{\circ\mathrm{R}} > 2.6$. Thus, from this analysis based on the model of Σ_2 only, one can expect that the control with $\kappa'_{\circ\mathrm{R}} = 2.6$ shows better damping performance than for $\kappa'_{\circ\mathrm{R}} = 5.0$. To see this, we calculate the transient response of the entire power system for the above fault. Fig. 5(c) shows the trajectories of the stator current. It can be seen that the controller with the smaller gain damps the oscillations much better than that with the higher gain. The fluctuations of the DC-link voltages are also sufficiently suppressed. These results demonstrate that the controller tuning can be easily done based on the local model of the wind farm.

V. Conclusion

The main contribution of this paper was to reveal three facts - first, DFIGs have resonant and uncontrollable modes depending on the ratio of their leakage reactance to resistance; second, adding a B2B converter in the stator line can be an effective way to overcome this difficulty; and third, this converter allows the closed-loop system including the grid dynamics to have a cascade structure where the grid affects the DFIG but not vice versa. We showed the effectiveness of the proposed approach through the IEEE 68-bus model with one wind farm. The proposed strategy can be an effective way of ensuring resilience of the grid as more wind power gets integrated over time. One drawback of the approach is the cost of adding the second B2B converter. This cost, however, is justified by return benefits as the B2B controller will enable much higher penetration levels for wind than what we have today without running into adverse issues caused by resonance and transient instability [4]. Moreover, with the development of solid-state technology [17], the cost of power-electronic converters is envisioned to reduce significantly in the foreseeable future. Therefore, we envision the proposed technology to be a cost-effective solution for large-scale wind integration.

References

[1] B. Kroposki, B. Johnson, Y. Zhang, V. Gevorgian, P. Denholm, B.-M. Hodge, and B. Hannegan, "Achieving a 100% renewable grid: Operating electric power systems with extremely high levels of variable renewable energy," *IEEE Power and Energy Magazine*, vol. 15, no. 2, pp. 61–73, 2017.

[2] C. E. Ugalde-Loo, J. B. Ekanayake, and N. Jenkins, "State-space modeling of wind turbine generators for power system studies," *IEEE Trans. on Industry Applications*, vol. 49, no. 1, pp. 223–232, 2013.

[3] E. Vittal, M. O'Malley, and A. Keane, "Rotor angle stability with high penetrations of wind generation," *IEEE Trans. on Power Systems*, vol. 27, no. 1, pp. 353–362, 2011.

[4] D. Gautam, V. Vittal, and T. Harbour, "Impact of increased penetration of dfig-based wind turbine generators on transient and small signal stability of power systems," *IEEE Trans. on power systems*, vol. 24, no. 3, pp. 1426–1434, 2009.

[5] V. Vittal and R. Ayyanar, *Grid Integration and Dynamic Impact of Wind Energy*. Springer-Verlag New York, 2013.

[6] Z. Miao, L. Fan, D. Osborn, and S. Yuvarajan, "Control of DFIG-based wind generation to improve interarea oscillation damping," *IEEE Trans. on Energy Conversion*, vol. 24, no. 2, pp. 415–422, 2009.

[7] Y. Xia, M. Yin, C. Cai, B. Zhang, and Y. Zou, "A new measure of the degree of controllability for linear system with external disturbance and its application to wind turbines," *Journal of Vibration and Control*, vol. 24, no. 4, pp. 739–759, 2018.

[8] E. D. Castronuovo, J. Martínez-Crespo, and J. Usaola, "Optimal controllability of wind generators in a delegated dispatch," *Electric power systems research*, vol. 77, no. 10, pp. 1442–1448, 2007.

[9] S. Riverso, F. Sarzo, and G. Ferrari-Trecate, "Plug-and-play voltage and frequency control of islanded microgrids with meshed topology." *IEEE Trans. on Smart Grid*, vol. 6, no. 3, pp. 1176–1184, 2015.

[10] F. Dörfler, J. W. Simpson-Porco, and F. Bullo, "Plug-and-play control and optimization in microgrids," in *Proc. of Conference on Decision and Control*. IEEE, 2014, pp. 211–216.

[11] O. Anaya-Lara, D. Campos-Gaona, E. Moreno-Goytia, and G. Adam, *Offshore wind energy generation: control, protection, and integration to electrical systems*. John Wiley & Sons, 2014.

[12] A. Petersson, T. Thiringer, L. Harnefors, and T. Petru, "Modeling and experimental verification of grid interaction of a dfig wind turbine," *IEEE Transactions on Energy Conversion*, vol. 20, no. 4, pp. 878–886, 2005.

[13] B. Pal and B. Chaudhuri, *Robust control in power systems*. Springer Science & Business Media, 2006.

[14] V. Akhmatov and H. Knudsen, "An aggregate model of a grid-connected, large-scale, offshore wind farm for power stability investigations - importance of windmill mechanical system," *International Journal of Electrical Power & Energy Systems*, vol. 24, no. 9, pp. 709–717, 2002.

[15] T. Sadamoto, A. Chakrabortty, T. Ishizaki, and J. Imura, "Dynamic modeling, stability, and control of power systems with distributed energy," *IEEE Control System Magazine*, vol. 39, no. 2, pp. 34–65, 2019.

[16] M. Vidyasagar, "Decomposition techniques for large-scale systems with nonadditive interactions: Stability and stabilizability," *IEEE Trans. on Automatic Control*, vol. 25, no. 4, pp. 773–779, 1980.

[17] F. Blaabjerg and K. Ma, "Future on power electronics for wind turbine systems," *IEEE Journal of Emerging and Selected Topics in Power Electronics*, vol. 1, no. 3, pp. 139–152, 2013.